OCEANOGRAPHY

Submesoscale-selective compensation of fronts in a salinity-stratified ocean

Gualtiero Spiro Jaeger[1,2]* and Amala Mahadevan[1]

Salinity, rather than temperature, is the leading influence on density in some regions of the world's upper oceans. In the Bay of Bengal, heavy monsoonal rains and runoff generate strong salinity gradients that define density fronts and stratification in the upper ~50 m. Ship-based observations made in winter reveal that fronts exist over a wide range of length scales, but at O(1)-km scales, horizontal salinity gradients are compensated by temperature to alleviate about half the cross-front density gradient. Using a process study ocean model, we show that scale-selective compensation occurs because of surface cooling. Submesoscale instabilities cause density fronts to slump, enhancing stratification along-front. Specifically for salinity fronts, the surface mixed layer (SML) shoals on the less saline side, correlating sea surface salinity (SSS) with SML depth at O(1)-km scales. When losing heat to the atmosphere, the shallower and less saline SML experiences a larger drop in temperature compared to the adjacent deeper SML on the salty side of the front, thus correlating sea surface temperature (SST) with SSS at the submesoscale. This compensation of submesoscale fronts can diminish their strength and thwart the forward cascade of energy to smaller scales. During winter, salinity fronts that are dynamically submesoscale experience larger temperature drops, appearing in satellite-derived SST as cold filaments. In freshwater-influenced regions, cold filaments can mark surface-trapped layers insulated from deeper nutrient-rich waters, unlike in other regions, where they indicate upwelling of nutrient-rich water and enhanced surface biological productivity.

INTRODUCTION

Lateral and vertical gradients in the upper ocean's density, namely, fronts and stratification, play an important role in upper ocean dynamics. Vertical stratification governs the depth and stability of the surface mixed layer (SML) and the behavior of internal waves and eddies. Fronts, or lateral density variations, give rise to baroclinic instability and eddies that convert potential energy to kinetic energy in the ocean, resulting in the conversion of horizontal density gradients to stratification. In regions that are nutrient-limiting for phytoplankton growth, fronts can enhance vertical supply of nutrients (*1*), whereas in light-limited regions, frontal slumping can enhance stratification and light exposure for phytoplankton (*2*). In much of the world's upper oceans, temperature variations govern the spatial gradients and seasonal variations of density, whereas salinity plays a secondary role (*3*). Sea surface temperature (SST) derived from satellites is therefore an indicator of ocean dynamics and reveals fronts, filaments, and eddies at scales of O(1 to 10) km. In temperature-stratified regions, surface cooling destabilizes the density stratification and causes a deepening of the SML and entrainment of subsurface waters that are relatively rich in nutrients. In general, cold SST features are interpreted as upwelled or vertically mixed waters that are nutrient-rich and support phytoplankton productivity.

However, in regions that are strongly influenced by freshwater runoff and rain or have close-to-freezing surface temperatures, salinity variations can be the leading control on near-surface density gradients (*4*, *5*). In these regions, the near-surface layer's response to atmospheric cooling differs from regions where the density of the SML is temperature-controlled. Here, density stratification is controlled by salinity, and the depth of the SML is defined by the vertical salinity gradient, so temperature can remain uniform (or even increase) with depth beneath the SML in the so-called barrier layer. By losing heat to the atmosphere, the SML can become colder than layers that lie subsurface, while still remaining stably stratified because of salinity (*6*). Areas of the SML that cool the most by heat loss to the atmosphere are those with the shallowest and strongest salinity stratification.

Although lateral density gradients or fronts occur over a wide range of scales, kilometer-scale fronts within the SML of the ocean form submesoscale instabilities and mixed-layer eddies that promote the downscale cascade of energy (*7*) while converting lateral buoyancy gradients into mixed-layer stratification. Such a process of restratification of the mixed layer by submesoscale baroclinic instability has been recently modeled and observed in a number of contexts (*2*, *8*). Because of the slumping of horizontal density gradients, the shallowest and strongest stratification forms along the edges of eddies and frontal instabilities, which also exhibit the strongest horizontal density gradients. The density stratification arising from salinity-controlled fronts is also salinity-controlled and not convectively unstable when cooled from above. Thus, when cooled by the atmosphere, the restratifying frontal regions experience a greater drop in SST than their surroundings (Fig. 1). This delineates them as cold filaments in satellite imagery. These cold filaments in salinity-controlled regions differ crucially from those in temperature-controlled regions. They emerge along submesoscale fronts where restratification by slumping cuts off communication with the subsurface.

An important facet of salinity-controlled density fronts in the SML is that they become temperature-compensated by atmospheric cooling where they restratify (Fig. 1). This occurs at kilometer scales where lateral density gradients are dynamically unstable within the SML and submesoscale in character. In what follows, we use high-resolution measurements of upper ocean temperature and salinity from the Bay of Bengal (BoB) in the Indian Ocean to reveal the scale-selective compensation of fronts that is observed in winter. We then use a process study model to demonstrate the underlying mechanism for the observed phenomenon. Finally, we discuss the prevalence and implications of the phenomenon.

[1]Woods Hole Oceanographic Institution, Woods Hole, MA 02543, USA. [2]Massachusetts Institute of Technology, Cambridge, MA 02139, USA.
*Corresponding author. Email: gvsj@mit.edu

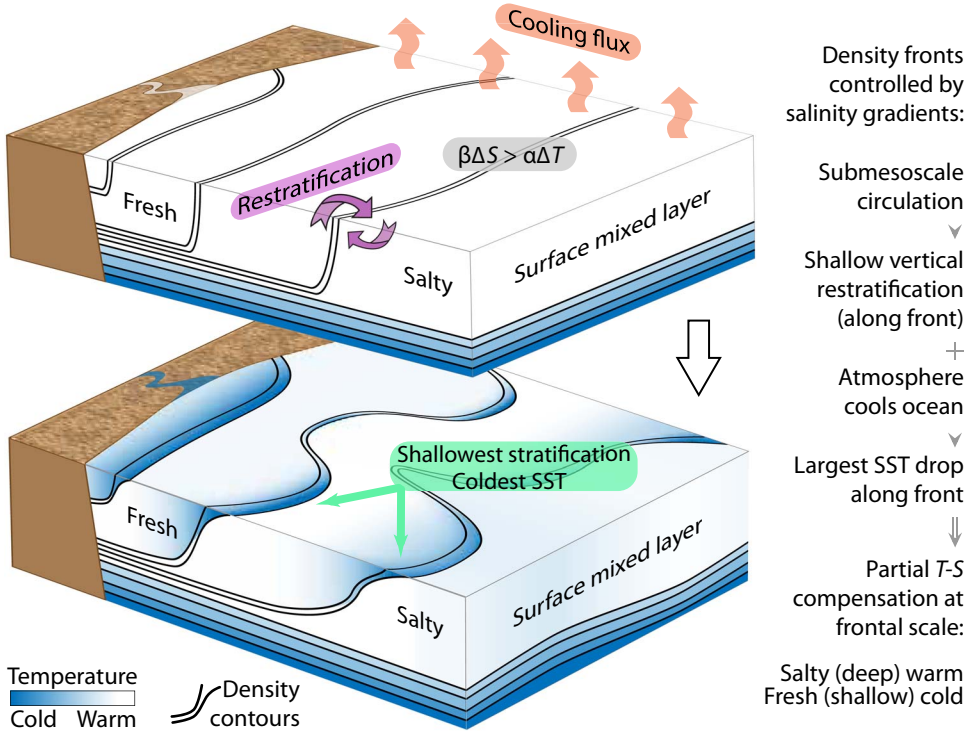

Fig. 1. Schematic drawing of the mechanism by which cooling creates density-compensated submesoscale fronts and cold SST filaments. In a salinity-stratified upper ocean, submesoscale instabilities of salinity fronts cause restratification and shallowing of the SML. Cooling is concentrated within shallow (most stratified) SMLs, creating a larger drop in SST along salinity-stratified fronts, at scales of submesoscale restratification. SST and SSS become correlated (salty warm and fresh cold, compensating their effects on density) at length scales ~O(1) km.

MATERIALS AND METHODS

Remote observations

The BoB is an exceptionally fresh, tropical ocean, receiving a large (circa 1.5 m/year) net input of fresh water from monsoonal rains and runoff (*9*, *10*). Although the surface waters are warm (~25° to 30°C on average), the depth and dynamics of the SML are strongly controlled by salinity (*11*). Large riverine inputs along the northern margins of the basin result in strong lateral salinity gradients that form density fronts within the SML (*6*). The fresher water, being less dense, forms a shallow SML with the vertical density gradient beneath the SML defined by the gradient in salinity (*12*). In many areas, we can observe a barrier layer, or layer between the halocline (which defines the depth of the SML) and thermocline (which defines the base of the isothermal layer) (*13*).

Contrasting behaviors can be seen in the Arabian Sea (AS) and BoB, the two northernmost regions of the Indian Ocean that flank the Indian subcontinent to the west and east. By early December, the seasonal surface winds over the northern Indian Ocean blow steadily from the northeast, advecting relatively dry and cool continental air over the AS and the BoB. This leads to a loss of heat and moisture to the atmosphere, cooling the sea surface [based on NASA Aquarius data (Fig. 2A) (*14*); NASA MODIS (Moderate Resolution Imaging Spectroradiometer) data (Fig. 2, B and D); NCEP GODAS (National Centers for Environmental Prediction Global Ocean Data Assimilation System) reanalysis (Fig. 2C) (*15*)]. Although SSTs in these two embayments span a similar range (24° to 29°C) at this time, their sea surface salinities (SSSs) are very different. SSS in the AS is between 36 and 37 practical salinity units (psu), whereas in the fresher BoB, it varies between 28 and 34 psu. Taking into account the relative magnitudes of the thermal expansion and haline contraction coefficients, these SST and SSS fields show that horizontal density gradients within the SML are controlled by temperature in the AS but by salinity in the BoB.

In the AS, the cold SST is correlated with high chlorophyll in the ocean color imagery from a satellite, which is indicative of vertical mixing or upwelling of nutrients from the subsurface. Entrainment of deeper colder (denser) waters into the SML lowers the SST and also leads to higher biological productivity in the AS (*16*).

A similar cold and biologically productive patch is seen in the BoB off the east coast of India because of vigorous mixing caused by the cyclonic storm Madi, which was active between December 6th and 13th (track marked in Fig. 2C). However, the cold SST features in the open bay north of 16°N lack any chlorophyll signature. These low SST regions in the northern BoB are not denser than their surroundings and are not formed because of vertical mixing or upwelling. The cooler water near surface is held up by salinity stratification as will be shown from in situ data (Fig. 2B). Whereas the scale of these cold SST patches and filaments is barely resolved by Aquarius SSS, it is better resolved by the newly available 1/4° Soil Moisture Active Passive satellite–derived SSS maps. In a representative snapshot of the northern BoB during the winter of 2015, we find that cold and fresh patches are generally colocated (fig. S1). In addition to the coldest water found at the northern coastline where the fresh river discharge enters the bay, cold filaments also appear along the front where the freshest water meets saltier water in the eastern BoB.

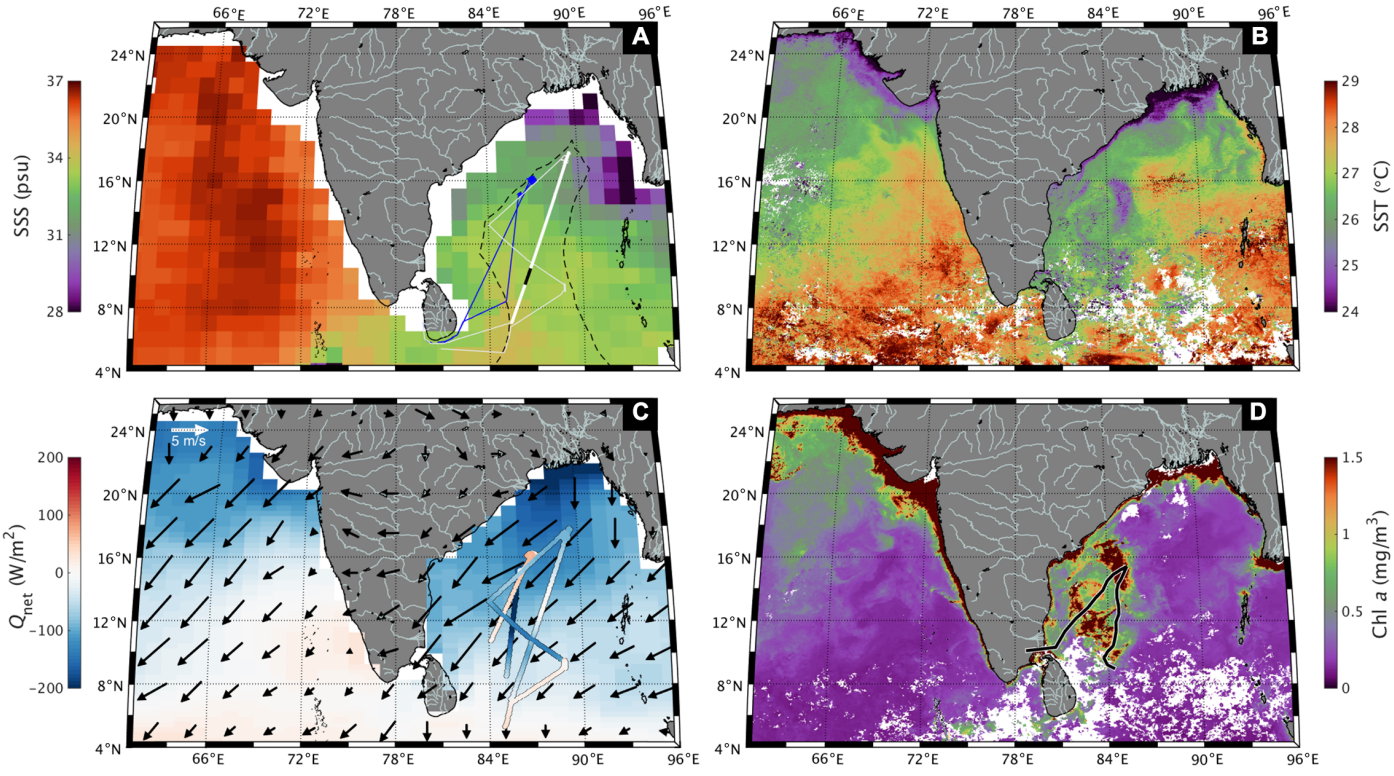

Fig. 2. Winter-monsoon sea surface conditions in the northern Indian Ocean (west, AS; east, BoB). (**A**) Surface salinity (November to December 2013, Aquarius satellite data). Thin lines mark the ship's track from 10 to 26 November (blue) and from 28 November to 13 December (white). Thick segments correspond to sections shown in Fig. 3. The dashed line marks the limits of international waters. (**B**) Nighttime SST (11 to 18 December, MODIS). (**C**) Net heat flux and surface winds (November to December 2013, NCEP reanalysis). Colored track show net daily heat flux measured during the surveys. (**D**) Chlorophyll *a* (Chl *a*) (25 November to 26 December, MODIS); track of the cyclonic storm Madi (6 to 13 December, Joint Typhoon Warning Center) shown in black. Dates of satellite data composites are chosen to provide a cloud-free view during the ship survey period.

Further insight into the relationship between salinity (S) and temperature (T) is provided by a detailed view of the hydrography obtained by conducting a high-resolution survey of the BoB from the *R/V Roger Revelle* in 2013.

Ship-based observations

Surface and subsurface salinity and temperature fields during the Northeast Monsoon were measured in two surveys between 10 to 26 November and 29 November to 11 December 2013. The surveys accomplished six transects between 5° and 18°N, the longest of which was about 1200 km long (Fig. 2). Underway conductivity-temperature-depth (UCTD) profiles taken at fairly regular intervals (averaging 5 km in separation during the straight transects of the second survey) show a fresh near-surface layer above a strong halocline that lies between 30- and 50-m depths. Temperature is generally inverted within this surface layer, but the vertical density gradient is kept stable by salinity stratification. Figure 3 shows a 100-km-long section of temperature, salinity, and density stratification (characterized by buoyancy frequency $N^2 \equiv \frac{-g}{\rho_o}\frac{\partial \rho}{\partial z}$, where ρ is the density, ρ_o is the reference density, and g is the acceleration due to gravity). The observed temperature inversion can be ascribed to the net air-sea heat flux of −50 W/m^2 (mean) computed from bulk meteorological measurements during the survey. The net flux is the sum of latent (−120 W/m^2), longwave (−50 W/m^2), and sensible (−10 W/m^2) mean negative components that exceed the mean solar shortwave (+130 W/m^2) warming flux. The dominant latent and shortwave components varied with wind speed, humidity, and cloud cover variations, whereas the variability of SST being less than 1°C had a comparatively small effect. Because the time scale and length scale of these atmospheric patterns are fast and large compared to submesoscale ocean processes (a mean wind speed of 7 m/s covers 600 km in a day), the net heat flux is considered uniform for our analysis.

Although the spacing of UCTD profiles allowed fronts wider than O(10) km to be resolved, the ship's flow-through thermosalinograph (TSG) system measured the T and S of water continuously pumped from a hull intake every 15 s. Because of the ship's displacement and disturbance of the surrounding water, these measurements are representative of the top 5 m of the ocean, which lies above the mean SML depth as diagnosed from the UCTD profiles. At a cruising speed of 11 knots, this sampling corresponds to a resolution of about 0.1 km. The TSG thus fully resolves length scales of O(1) km, enabling us to observe submesoscale (kilometer-scale) horizontal gradients and features in the SML (Fig. 3).

Horizontal gradients of density (or buoyancy) within the SML are dominated by S, whereas T is nearly uniform. The data in Fig. 3A are plotted such that equal vertical excursions along the T and S axes represent equal changes in density, albeit of opposite sign, as in the study of Rudnick and Ferrari (*17*). Although horizontal density-scaled temperature gradients in the SML are negligible compared to salinity gradients at large scales, they become comparable at scales of a few kilometers, with temperature partially compensating salinity's control

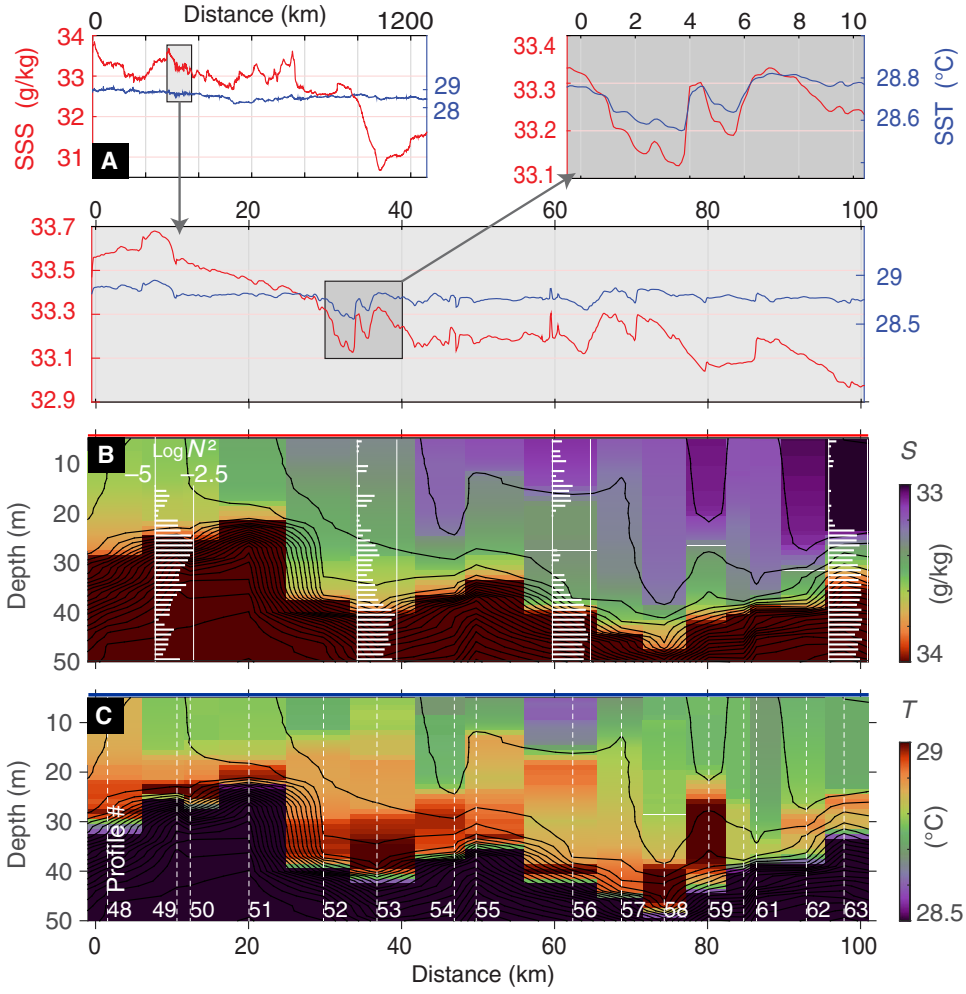

Fig. 3. Surface-layer salinity and temperature structure in the BoB observed between 29 November and 3 December 2013. (**A**) 1200 km south-to-north transect (marked on map) of surface salinity (red) and temperature (blue) from a shipboard TSG. Shaded boxes show a 100- and 10-km section in detail. The ranges of vertical *T* and *S* axes are proportionally scaled by the thermal expansion and haline contraction coefficients α and β, such that graphically equal displacements have equal effect on density. Compensating correlation is seen at scales below O(10) km. (**B**) Salinity and (**C**) temperature section composed of UCTD profiles (numbered, dashed vertical lines) taken during the 100-km section plotted above. Density (in black contours) and a few profiles of stratification (log N^2 indicated by white bar graphs) are overlaid. Note the cooler surface waters confined above warmer subsurface layers by stable salinity stratification.

of lateral density variations at scales of O(1) km. This pattern of *T*-*S* coherence at small scales is seen not only in this highlighted section but throughout the entire survey.

Analysis

To quantify the relative importance of the horizontal temperature and salinity gradients on the horizontal density gradients (frontal intensity), we calculate the density ratio, $R = \alpha\Delta T/\beta\Delta S$, and related Turner angle (Tu = arctan *R*) (*18*), where ΔT and ΔS are the horizontal variations of *T* and *S* between two points along track and α and β are the thermal and haline expansion coefficients calculated at the measured *T* and *S*. $|R| < 1$ indicates that salinity gradients are more important than temperature gradients in setting the density gradient, and the opposite is true for $|R| > 1$. Positive *R* indicates compensating *T* and *S* effects on density. At $R = 1$, equal and opposite *T* and *S* gradients cancel out any density variation. The mapping of *R* onto Tu is chosen such that the origins coincide and Tu ranges between $\pm \pi/2$ (Fig. 4). Following the study of Rudnick and Martin (*19*), our analysis is performed with Tu because Tu, unlike *R*, is confined to a finite range, but the results are described using the corresponding, and more intuitive, *R* values.

For each of the six survey sections, we perform a wavelet decomposition of *T* and *S* to separate the gradients by spatial scale as in the study of Rudnick and Ferrari (*17*), which is in effect similar to a series of band-pass filters. At each level (scale) of the *T* and *S* decomposition, finite differences between adjacent wavelet coefficients are used to calculate *R*, yielding a gradient scale–specific distribution of density ratios (more details available in the Supplementary Materials). The histograms of *R* at 100-, 10-, and 1-km scales (black curves in Fig. 4A) from the 1200-km-long section shown in Fig. 3A reveal a narrow peak around $R = 0$ at the large (~100 km) scale. However, the peak of the distribution is shifted toward positive *R* at 10-km scales and even more so at 1-km scales. At this smallest resolved scale, the strongest fronts are salinity-controlled and partially compensated by temperature so that *R* lies between 0 and 1 with a median of 0.3.

The distributions of *R* include segments where both *T* and *S* gradients happen to be negligibly small (fig. S2), yielding some very large

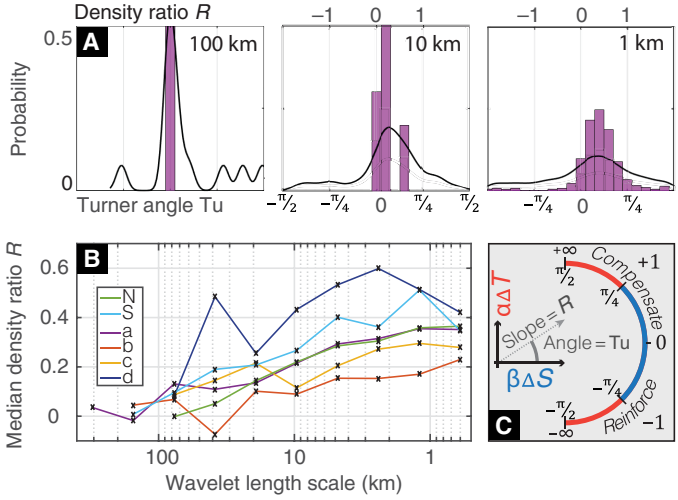

Fig. 4. Scale dependence of *T*-*S* compensation. (**A**) Probability distributions of *R* (density ratio) for different horizontal gradient scales, 100, 10, and 1 km, as estimated from the longest ship section (leg 2, section A in previous figures). Black lines show the distribution of *R* for all gradients, whereas purple bars denote the distribution of *R* for only the largest gradients (selected as the 95th percentile of individual $\alpha\Delta T$ or $\beta\Delta S$ magnitudes shown in fig. S2). Density compensation of fronts is greater at 10-km scales than 1000-km scales and greater at 1-km scales than 10-km scales ($R = 1$ and $\mathrm{Tu} = \pi/4$ denote perfect compensation). (**B**) Median of *R* distribution as a function of horizontal length scale for each of the six ship transects. Pairs of $\alpha\Delta T$ and $\beta\Delta S$ are computed from a wavelet decomposition of the individual ship transects mapped in Fig. 2A. Lines (N) and (S) are from the earlier cruise, and lines (a) to (d) are from the later cruise, both during November to December 2013. All transects are consistent in showing that greater density compensation is favored at smaller scales. (**C**) Schematic demonstrating the relationship between density ratio $R = \alpha\Delta T/\beta\Delta S$ and Turner angle Tu.

magnitudes of *R* that make the distributions long-tailed (black curves in Fig. 4A). To highlight just the strongest *T* and *S* fronts, we select for the largest 5% of individual $\alpha\Delta T$ and $\beta\Delta S$ gradients shown as discrete bars in the histogram (Fig. 4A). These agree with the distributions that include both strong and weak fronts (black lines) but show an even narrower range of *R* confined between 0 and 1.

All ship transects are consistent in showing that greater density compensation is favored at smaller scales of O(1) km. The medians of the distributions are near 0 at large O(100)-km scales but positive (between 0 and 1) at smaller scales. In other words, *T* gradients are negligible at large scales but increasingly compensate *S* gradients at the submesoscale. The transect showing the greatest compensation at all scales (leg 2, transect D) is anomalous because it was taken after the cyclonic storm Madi passed over the southern BoB in early December.

A previous study of the *T*-*S* relationship (*20*) in the subtropical Pacific found that the *T* and *S* gradients in the SML compensate each other at all scales ranging from 1000 km to 10 m. Distributions of density ratios, calculated at scales of 10, 1, 0.1, and 0.02 km, were all centered around $R = 1$, independent of the length scale. The authors' explanation for the scale-independent predominance of compensation is that although stochastic forcing can create *T* and *S* gradients with a broad distribution of density ratios at the scale of the surface buoyancy forcing, any uncompensated *T* or *S* gradient ($R \neq 1$) is a density front, which is dynamically active and is dissipated or mixed away. However, a compensated *T*-*S* gradient ($R = 1$) has no density signature (although it has a gradient in the passive tracer "spice") and is thus not dynamically active. Instead, it can be stirred by eddies to finer and finer scales, while maintaining the same R (=1) as the larger-scale gradient from which it originated. Other studies have continued to examine *T*-*S* compensation in open-ocean settings, finding compensation on 3 to 4 km scales in all oceans when the SML is deep but not when the SML is shallow (*19*). Both compensated and uncompensated gradients are found at scales below 10 km in the North Pacific Subtropical Front (*21*).

However, the observation in the BoB of an abundance of partially compensated salinity-dominated fronts ($0 < R < 1$) and a relative absence of temperature-dominated fronts partially compensated by salinity ($R > 1$) is not explained by stochastic forcing. The scale dependence of the observed correlation cannot be ascribed to the downscale cascade of larger-scale compensation by stirring because, here, the larger-scale gradients are uncompensated and compensation increases with decreasing length scales both from 100 to 10 km and from 10 to 1 km. Furthermore, although density (salinity) fronts are observed at all scales, they are either uncompensated or partially compensated, but none of the strongest fronts are reinforced by temperature gradients acting in concert with the salinity gradient ($R < 0$).

We propose that the observed increased correlation of *T* with *S* at kilometer scales is the result of surface cooling of salinity gradient–dominated fronts (fig. S3). Mesoscale eddying processes of O(100) km stir and strain the large-scale salinity (density) gradients, sharpening fronts. Submesoscale instabilities acting on O(1 to 10) km scales (*22*) tend to slump these fronts through O(1) Rossby number processes, increasing shallow stratification beneath the lighter side of the front (*8*). Near-surface stratification is then positively correlated with the surface buoyancy at this scale, with increased density stratification occurring where the surface salinity is low. This means that the depth of the SML is also correlated with salinity gradients at kilometer scales. If the surface is now cooled by an air-sea heat flux that is smooth (uniform) over kilometer scales and the surface heat loss is distributed into the mixed layer, then the shallower and fresher side has a smaller heat capacity and will incur a greater drop in temperature than the deeper and saltier side. This forcing mechanism would tend to correlate *T* with *S*, moving *R* from 0 to 1 at the scale of frontal restratification.

This compensation mechanism is scale-selective for two reasons. First, at scales larger than the submesoscale, there are many competing processes affecting the depth of the SML that are unrelated to local horizontal surface density gradients. Thus, large-scale patterns of SML depths are not well correlated with SSS, and cooling does not necessarily lead to large-scale compensation of SST with SSS. Second, for a given heat flux, the largest SST response is achieved in the shallowest SMLs found at the sharpest fronts. Thus, even if both the large-scale SML-depth variations and the small-scale restratified SML-depth variations are correlated with SSS, density compensation by temperature will be first achieved at the sites of shallow stratification, which are submesoscale fronts.

Three-dimensional modeling

To demonstrate this mechanism creating scale-selective *T*-*S* compensation, we configured a nonhydrostatic, submesoscale permitting Process Study Ocean Model (PSOM) (*23*) within a periodic channel 48 km (along front) × 96 km (across front) to simulate a salinity front in the SML (upper 40 m), set above a pycnocline (Fig. 5). The front was initialized with a tanh cross-front salinity variation, connecting two vertical *S* profiles measured during the same BoB cruise as the

data in Fig. 3. Temperature T was initialized from the same profile but is horizontally uniform. This created an idealized, uncompensated salinity front, with realistic horizontal density gradients and vertical stratification. The model grid dimensions were 250 m in the horizontal (with 192 × 384 grid cells) and 1 m in the vertical near surface increasing with depth (64 levels). The numerical model is integrated with 1-min time steps. Subgrid processes were parameterized with a constant horizontal diffusivity of 0.2 m^2/s and the $\kappa - \epsilon$ turbulence closure scheme (*24*), as previously described (*25*). Additional model simulations were run with a 5- and 25-fold increase in horizontal diffusivity to 1 and 5 m^2/s, which lies within the observed range (*26*). The model was also run with half the horizontal grid resolution, but the results were insensitive to these parameter changes (figs. S4 and S5).

The density front was initially in thermal wind balance with a frontal jet, which became unstable and developed meanders and filaments within 1 week of model spin-up in which no surface forcing was applied. For the following week, the model was forced with a constant and uniform surface heat flux of −50 W/m^2 that cooled the ocean. In addition to the $\kappa - \epsilon$ scheme, a convective mixing scheme was used to rapidly distribute the buoyancy loss downward from the surface until static stability was achieved in the model.

MODEL RESULTS

The initially uniform SST field develops kilometer-scale features correlated with SSS gradients of O(1 to 10) km. The largest drop in

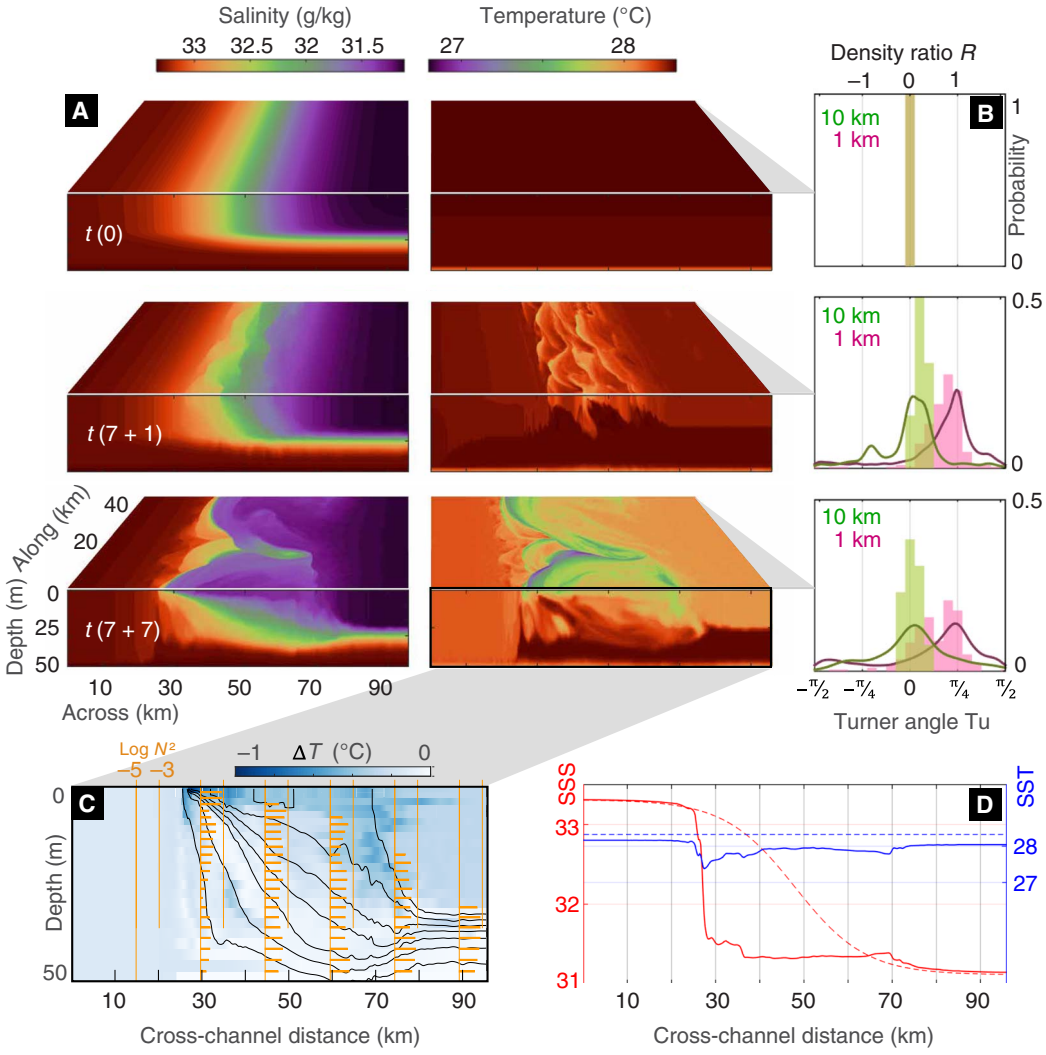

Fig. 5. Numerical simulation of a submesoscale salinity front forced by surface cooling, developing O(1)-km scale *T-S* compensation. (**A**) Surface- and depth-dependent salinity (left) and temperature (right) from our process study numerical ocean model, or PSOM, configured in a periodic channel. The model domain extends 10 times deeper than what is shown. Top: Model initial condition at $t = 0$ days. Middle: $t = 8$ days, comprising 7 days of model integration without any heat flux and 1 day of cooling by a constant and uniform surface heat flux of −50 W/m^2. Bottom: $t = 14$ days of which the last 7 days are with cooling. (**B**) Distributions of surface density ratio R, initially (top), after 1 day of cooling (middle), and after 1 week of cooling (bottom). Filtering for horizontal gradient scales of order 10 km (pale green) and 1 km (pink). Lines show distributions for ratios of all gradients, whereas shaded bars show distributions for ratios of only the largest T and S gradients, as in Fig. 4. (**C**) Temperature change (of a cross-channel section) after 1 week of surface cooling. Isopycnals (black contours) and stratification (yellow bars). (**D**) SSS (red) and SST (blue) across the section initially (dashed line) and after the front evolves and is cooled for 1 week (solid line).

SST is found along the sharpest fronts, which in time, become cold filaments in SST. These cold filaments are not dense filaments connected to deeper colder waters, but rather, they mark an increased near-surface stratification forming extremely shallow SMLs on the less dense side along fronts. A vertical section through the model domain shows heat trapped beneath the cold fresh side of fronts; the temperature inversion is kept stable by the strong salinity stratification (Fig. 5C). On the domain scale, the differences in initial SML depths between the fresher side (25 m) and the saltier side (50 m) lead to a large-scale correlation (albeit weaker than the small-scale correlation) of SST with SSS because the uniform heat loss is confined to a shallower versus a deeper SML. A control run of the model without surface cooling develops similar salinity fronts and kilometer-scale features, but the salinity fronts remain uncompensated because the surface temperature remains uniform (fig. S6).

We repeated our scale-selective analysis of density ratio distributions on a series of cross-channel surface transects from the model output (Fig. 5B). Within 1 day of cooling, the initially uniform density ratio ($R = 0$) at both the 10- and 1-km scales develops into a broader distribution of R shifted toward positive values. After 1 week of cooling, the median R value of strong fronts in the model is equal to 0.57 [for O(1) km scales] and 0.06 [for O(10) km scales], compared to 0.31 and 0.16, respectively, in the TSG data. The interquartile range of the O(1) km strong fronts falls between $R = 0.19$ and 0.86 in the model and $R = 0.15$ and 0.52 in the TSG data. Similar to the *T*-*S* compensation observed in the BoB, the model exhibits compensation preferentially at smaller scales.

DISCUSSION

Besides horizontal compensation, the greater temperature drop along the front also brings fresher water to the same density as slightly saltier but warmer water. Any along-isopycnal subduction of water at the front then increases the salinity variance along isopycnals, and isopycnal stirring and mixing can disperse the fresh water into saltier deeper layers. Simply put, the increased heat loss (buoyancy loss) of fresher water, compared to deeper saltier SMLs, decreases the density difference between fresh and salty water masses.

Geographic occurrence

The prevalence of such cooling-induced compensation can be estimated globally by identifying regions in which both necessary factors, a cooling flux and salinity-dominated gradients, are simultaneously met in the SML. Using a climatology of surface Q_{net} from OAFlux (*27*) and a climatology of horizontal density ratios, calculated from smoothed *T*-*S* gradients in the SML based on Monthly Isopycnal/Mixed-layer Ocean

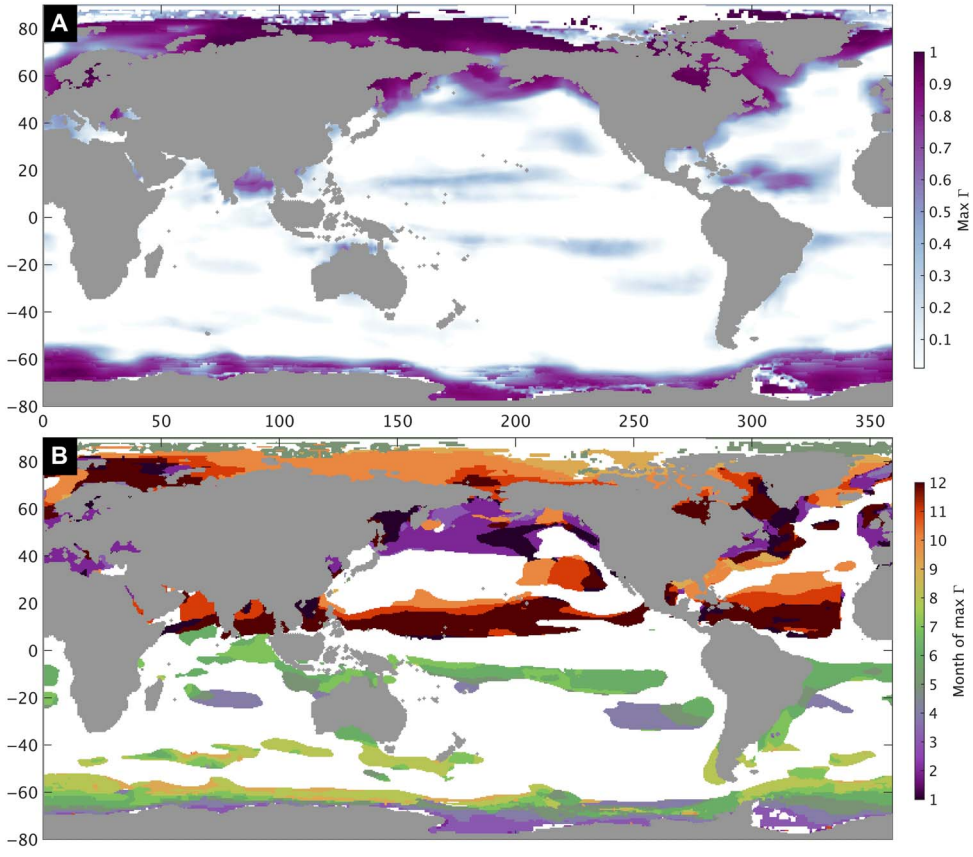

Fig. 6. Climatological estimate of the global prevalence of cooling-induced *T*-*S* compensation. (**A**) Possible occurrence of cooling-induced compensation where both the SML is cooled and density gradients are salinity-dominated. The estimate, cast as a likelihood between 0 and 1, is based on a co-occurrence of the necessary factors calculated from a climatology of surface heat flux and horizontal density ratios (normalized factors designated q and r), with greater weight placed on larger (negative) fluxes and stronger salinity control (smaller density ratio). The maximum ($\Gamma = q \cdot r$) of the 12 months for each pixel is plotted in (A), and darker shades indicate more favorable conditions. (**B**) Month of the maximum Γ (1 = January, 12 = December), generally corresponding to local winter months.

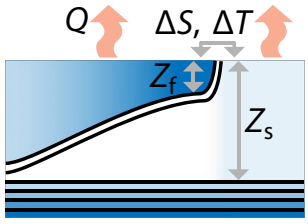

Fig. 7. Idealized SSS submesoscale front, where the shallow restratification is due to the slumping of the lateral salinity gradient. Temperature is shaded in color, and contours of density are in black.

Climatology (*3*), a database of global SML salinity and temperature objective maps, we estimate the likelihood of these conditions being met in the ocean for each month of the year, placing greater weight on larger (negative) fluxes and stronger salinity control (smaller density ratio). For each 1° × 1° ocean pixel, we calculate two normalized factors, $q = \frac{-Q_{net}}{50\ W/m^2}$ and $r = \frac{45^\circ - |Tu|}{45^\circ}$, assigning 0 to negative values and limiting positive values to 1. The product $\Gamma(x, y, t) = q \cdot r$ is an estimate for the occurrence of cooling-induced compensation for each month. The maximum value across all months is mapped in Fig. 6, along with the respective month of occurrence. Besides confirming the BoB's favorable conditions, these factors predict the mechanism to potentially be active in the polar oceans and coastal seas, especially at higher latitudes, covering 20% of the global ocean (where $\Gamma > 0.5$ in any month). These factors are based on climatological monthly mean fluxes. However, shorter periods of intense cooling can also compensate SSS gradients, and hence, this analysis provides a conservative estimate. Enhanced *T*-*S* correlation at small scales is expected in regimes where large-scale salinity gradients create density fronts and the atmosphere cools the surface (such as coastal oceans with an active input of fresh water during fall and winter or polar seas). In regions of weak salinity gradients, such as the subtropical open oceans, this mechanism is not supported, and *T*-*S* compensation is not expected to be enhanced at kilometer scales.

Compensation time scale

Dynamics at the submesoscale are thought to provide a crucial link between the large-scale energy input to the ocean and the scales of turbulent dissipation of energy (*28*). Whereas geostrophic turbulence causes energy to cascade to larger scales, ageostrophic frontal dynamics can convert baroclinic potential energy to kinetic energy at smaller scales. The kilometer-scale horizontal density gradients powering these circulations are controlled by *T* and *S*. Here, we show that submesoscale-selective density compensation can weaken these fronts, forestalling the release of submesoscale energy to smaller scales through which dissipation can occur.

As a measure of the mechanism's importance in a given regime, we estimate the nondimensional density ratio $\left(R = \frac{\alpha \Delta T}{\beta \Delta S}\right)$ attained within the dynamical time scale of an inertial period ($2\pi/f$) by an initially uncompensated ($R = 0$) salinity front (ΔS) forced by a time-mean cooling flux (Q). If the restratified SML depth (z_f) is less than the SML depth on the salty side (z_s), the front changes more rapidly in temperature $\left(\delta T = \frac{-Q \cdot 2\pi/f}{z \cdot c_p \cdot \rho_o}\right)$ where c_p and ρ_o are the specific heat capacity and the mean density of seawater, respectively, and z is the SML depth, on the fresher side than on the saltier side of the front (Fig. 7; for other cases, see fig. S7). This leads to a lateral temperature difference ($\Delta T = \delta T_s - \delta T_f$), which increases the density ratio to $R = \frac{2\pi \cdot Q \cdot \left(\frac{1}{z_f} - \frac{1}{z_s}\right)}{f \cdot c_p \cdot \rho_o \cdot \left(\frac{\beta}{\alpha}\right) \cdot \Delta S}$ within an inertial period.

As the across-front temperature difference increases toward fully compensating the salinity front, the vertical temperature inversion also compensates the vertical salinity restratification. Any further heat loss will cause a deepening of the fresh SML, mixing with warmer saltier water below the restratification, reducing the sharpness of the compensated salinity front and vertically redistributing the previously surface-trapped heat loss. Thus, the density ratio of these surface fronts tends toward 1 but does not exceed 1.

In general, the time scale to attain full compensation is longer than one inertial period. For example, a 0.5-psu salinity front at 20° latitude, with 10-m shallow restratification next to a 50-m-deep SML, will become 33% compensated within an inertial period forced by a cooling flux (150 W/m^2) and thus fully compensated within three inertial periods.

CONCLUDING REMARKS

Beyond demonstrating a source of *T*-*S* coherence at small scales, the findings point to the importance of considering salinity fields when interpreting SST. Commonly, SST gradients are interpreted as density gradients, and cold filaments are associated with dense water that is exchanged with the subsurface. However, in salinity-controlled regions, temperature fronts might actually be oppositely oriented density fronts (the colder side being more buoyant) that are controlled by salinity, and cold filaments may represent enhanced surface stratification instead of deeper mixed layers. In nutrient-poor regions, we would not expect enhanced phytoplankton productivity at these cold filaments, whereas in nutrient-rich but light-limited regions, we would expect enhanced biological growth in these types of cold shallow filaments.

Of further interest is the potential contribution that active surface compensation might make to the subduction of fresher water, water mass formation, and enhancement of isopycnal *T*-*S* variance or spice that can be stirred along isopycnals. Submesoscale fronts are ubiquitous in the ocean and are important for the cascade of tracer variance and energy from large-scale forcing to scales where they are dissipated. Submesoscale fronts are also associated with significant localized vertical velocities, connecting the surface with subsurface waters. Our analysis of observations and numerical modeling show that in regions where salinity defines the density gradients, surface cooling leads to the selective weakening of submesoscale density fronts by *T*-*S* compensation and forms cold SST filaments at the most stratified submesoscale frontal boundaries.

SUPPLEMENTARY MATERIALS

Supplementary material for this article is available at http://advances.sciencemag.org/cgi/content/full/4/2/e1701504/DC1

section S1. Satellite data

section S2. Compensation between salinity and temperature for fronts of varying strength

section S3. Density compensation at a salinity front illustrated in a one-dimensional framework

section S4. Model sensitivity tests

section S5. Vertical density compensation: Weakening the density stratification by cooling

table S1. Parameter configuration space of sensitivity tests.

fig. S1. Similar to Fig. 2 but for winter 2015.

fig. S2. Scatterplots of density variability at a wavelength of 0.6 km due to salinity and temperature gradients along the longest straight section from the cruise (leg 2, section A).

fig. S3. Illustration of active compensation and creation of spice variance with a series of one-dimensional column models.
fig. S4. Simulations assessing the model's sensitivity to the value of horizontal diffusivity, set at 0.2, 1.0, and 5.0 m^2/s.
fig. S5. Tests assessing the sensitivity of the simulation to the horizontal grid resolution, set at 0.25 and 0.5 km, for the same domain (48 × 96 km) and the same value of horizontal diffusivity (1.0 m^2/s).
fig. S6. Tests assessing model evolution with no surface cooling, as well as with surface cooling during model spin-up.
fig. S7. Schematic showing variants of simple salinity fronts and stratification.

REFERENCES AND NOTES

1. M. Lévy, P. Klein, A.-M. Treguier, Impact of sub-mesoscale physics on production and subduction of phytoplankton in an oligotrophic regime. *J. Mar. Res.* **59**, 535–565 (2001).
2. A. Mahadevan, E. D'Asaro, C. Lee, M. J. Perry, Eddy-driven stratification initiates north atlantic spring phytoplankton blooms. *Science* **337**, 54–58 (2012).
3. G. C. Johnson, S. Schmidtko, J. M. Lyman, Relative contributions of temperature and salinity to seasonal mixed layer density changes and horizontal density gradients. *J. Geophys. Res. Oceans* **117**, C04015 (2012).
4. M.-L. Timmermans, P. Winsor, Scales of horizontal density structure in the Chukchi Sea surface layer. *Cont. Shelf Res.* **52**, 39–45 (2013).
5. J. A. MacKinnon, J. D. Nash, M. H. Alford, A. J. Lucas, J. B. Mickett, E. L. Shroyer, A. F. Waterhouse, A. Tandon, D. Sengupta, A. Mahadevan, M. Ravichandran, R. Pinkel, D. L. Rudnick, C. B. Whalen, M. S. Alberty, J. S. Lekha, E. C. Fine, D. Chaudhuri, G. L. Wagner, A tale of two spicy seas. *Oceanography* **29**, 50–61 (2016).
6. A. Mahadevan, G. Spiro Jaeger, M. Freilich, M. M. Omand, E. L. Shroyer, D. Sengupta, Freshwater in the Bay of Bengal: Its fate and role in air-sea heat exchange. *Oceanography* **29**, 72–81 (2016).
7. X. Capet, P. Klein, B. L. Hua, G. Lapeyre, J. C. Mcwilliams, Surface kinetic energy transfer in surface quasi-geostrophic flows. *J. Fluid Mech.* **604**, 165–174 (2008).
8. B. Fox-Kemper, R. Ferrari, R. Hallberg, Parameterization of mixed layer eddies. Part I: Theory and diagnosis. *J. Phys. Oceanogr.* **38**, 1145–1165 (2008).
9. R. R. Rao, R. Sivakumar, Seasonal variability of sea surface salinity and salt budget of the mixed layer of the north Indian Ocean. *J. Geophys. Res. Oceans* **108**, 3009 (2003).
10. S. R. Shetye, A. D. Gouveia, D. Shankar, S. S. C. Shenoi, P. N. Vinayachandran, D. Sundar, G. S. Michael, G. Nampoothiri, Hydrography and circulation in the western Bay of Bengal during the northeast monsoon. *J. Geophys. Res. Oceans* **101**, 14011–14025 (1996).
11. D. Sengupta, G. N. Bharath Raj, M. Ravichandran, J. S. Lekha, F. Papa, Near-surface salinity and stratification in the north Bay of Bengal from moored observations. *Geophys. Res. Lett.* **43**, 4448–4456 (2016).
12. M. S. Girishkumar, M. Ravichandran, M. J. McPhaden, Temperature inversions and their influence on the mixed layer heat budget during the winters of 2006–2007 and 2007–2008 in the Bay of Bengal. *J. Geophys. Res. Oceans* **118**, 2426–2437 (2013).
13. V. P. Thangaprakash, M. S. Girishkumar, K. Suprit, N. S. Kumar, D. Chaudhuri, K. Dinesh, A. Kumar, S. Shivaprasad, M. Ravichandran, J. T. Farrar, R. Sundar, R. A. Weller, What controls seasonal evolution of sea surface temperature in the Bay of Bengal?: Mixed layer heat budget analysis using moored buoy observations along 90°E. *Oceanography* **29**, 202–213 (2016).
14. G. Lagerloef, F. Wentz, S. Yueh, H.-Y. Kao, G. Johnson, J. M. Lyman, Aquarius satellite mission provides new, detailed view of sea surface salinity. *Bull. Am. Meteorol. Soc.* **93**, S70–S71 (2012).
15. E. Kalnay, M. Kanamitsu, R. Kistler, W. Collins, D. Deaven, L. Gandin, M. Iredell, S. Saha, G. White, J. Woollen, Y. Zhu, A. Leetmaa, R. Reynolds, M. Chelliah, W. Ebisuzaki, W. Higgins, J. Janowiak, K. C. Mo, C. Ropelewski, J. Wang, R. Jenne, D. Joseph, The NCEP/NCAR 40-year reanalysis project. *Bull. Am. Meteorol. Soc.* **77**, 437–471 (1996).
16. S. P. Kumar, N. Ramaiah, M. Gauns, V. V. S. S. Sarma, P. M. Muraleedharan, S. Raghukumar, M. D. Kumar, M. Madhupratap, Physical forcing of biological productivity in the northern Arabian Sea during the northeast monsoon. *Deep Sea Res. II Top. Stud. Oceanogr.* **48**, 1115–1126 (2001).
17. D. L. Rudnick, R. Ferrari, Compensation of horizontal temperature and salinity gradients in the ocean mixed layer. *Science* **283**, 526–529 (1999).
18. B. Ruddick, A practical indicator of the stability of the water column to double-diffusive activity. *Deep Sea Res. A* **30**, 1105–1107 (1983).
19. D. L. Rudnick, J. P. Martin, On the horizontal density ratio in the upper ocean. *Dynam. Atmos. Oceans* **36**, 3–21 (2002).
20. R. Ferrari, D. L. Rudnick, Thermohaline variability in the upper ocean. *J. Geophys. Res. Oceans* **105**, 16857–16883 (2000).
21. P. Hosegood, M. C. Gregg, M. H. Alford, Sub-mesoscale lateral density structure in the oceanic surface mixed layer. *Geophys. Res. Lett.* **33**, L22604 (2006).
22. L. N. Thomas, A. Tandon, A. Mahadevan, Submesoscale processes and dynamics, in *Ocean Modeling in an Eddying Regime*, M. W. Hecht, H. Hasumi, Eds. (American Geophysical Union, 2008), pp. 17–38.
23. A. Mahadevan, J. Oliger, R. Street, A nonhydrostatic mesoscale ocean model. Part I: Well-posedness and scaling. *J. Phys. Oceanogr.* **26**, 1868–1880 (1996).
24. H. Burchard, K. Bolding, Comparative analysis of four second-moment turbulence closure models for the oceanic mixed layer. *J. Phys. Oceanogr.* **31**, 1943–1968 (2001).
25. S. Mukherjee, S. Ramachandran, A. Tandon, A. Mahadevan, Production and destruction of eddy kinetic energy in forced submesoscale eddy-resolving simulations. *Ocean Model.* **105**, 44–59 (2016).
26. A. Y. Shcherbina, M. A. Sundermeyer, E. Kunze, E. D'Asaro, G. Badin, D. Birch, A.-M. E. G. Brunner-Suzuki, J. Callies, B. T. Kuebel Cervantes, M. Claret, B. Concannon, J. Early, R. Ferrari, L. Goodman, R. R. Harcourt, J. M. Klymak, C. M. Lee, M.-P. Lelong, M. D. Levine, R.-C. Lien, A. Mahadevan, J. C. McWilliams, M. J. Molemaker, S. Mukherjee, J. D. Nash, T. Özgökmen, S. D. Pierce, S. Ramachandran, R. M. Samelson, T. B. Sanford, R. K. Shearman, E. D. Skyllingstad, K. S. Smith, A. Tandon, J. R. Taylor, E. A. Terray, L. N. Thomas, J. R. Ledwell, The LatMix summer campaign: Submesoscale stirring in the upper ocean. *Bull. Am. Meteorol. Soc.* **96**, 1257–1279 (2015).
27. L. Yu, X. Jin, R. A. Weller, "Multidecade global flux datasets from the objectively analyzed air-sea fluxes (OAFlux) project: Latent and sensible heat fluxes, ocean evaporation, and related surface meteorological variables," *OAFlux Project Tech. Rep.* (OA-2008-01) **74** (2008).
28. J. C. McWilliams, Submesoscale surface fronts and filaments: Secondary circulation, buoyancy flux, and frontogenesis. *J. Fluid Mech.* **823**, 391–432 (2017).

Acknowledgments: We are grateful to the captain and crew of the *R/V Roger Revelle*, co-chief scientist of the cruise E. L. Shroyer, and all ASIRI-OMM (Air-Sea Interaction Regional Initiative–Ocean Mixing and Monsoons) scientists, including A. Tandon, D. Sengupta, J. T. Farrar, R. A. Weller, M. M. Omand, A. F. Waterhouse, V. V. S. S. Sarma, and A. L. Gordon. **Funding:** This work was carried out under the Office of Naval Research's ASIRI (grants N000141612470 and N000141310451) in collaboration with the Indian Ministry of Earth Science's OMM initiative supported by the Monsoon Mission. **Author contributions:** G.S.J. performed the data analysis and modeling. A.M. contributed to the design of fieldwork, procurement of data, and the development of the model. The manuscript was written jointly, and both authors collaborated on the interpretation of data and conception of the experiments. **Competing interests:** The authors declare that they have no competing interests. **Data and materials availability:** All data needed to evaluate the conclusions in the paper are present in the paper and/or the Supplementary Materials. Additional data related to this paper may be requested from the authors.

Submitted 8 May 2017
Accepted 23 January 2018
Published 28 February 2018
10.1126/sciadv.1701504

Citation: G. Spiro Jaeger, A. Mahadevan, Submesoscale-selective compensation of fronts in a salinity-stratified ocean. *Sci. Adv.* **4**, e1701504 (2018).

Submesoscale-selective compensation of fronts in a salinity-stratified ocean

Gualtiero Spiro Jaeger and Amala Mahadevan

Sci Adv **4** (2), e1701504.
DOI: 10.1126/sciadv.1701504